View Article Online
View Journal

Nanoscale Horizons

The home for rapid reports of exceptional significance in nanoscience and nanotechnology

Accepted Manuscript

This article can be cited before page numbers have been issued, to do this please use: Q. Xue, Z. Li, Q. Wang, W. Pan, Y. Chang and X. Duan, *Nanoscale Horiz.*, 2020, DOI: 10.1039/D0NH00098A.

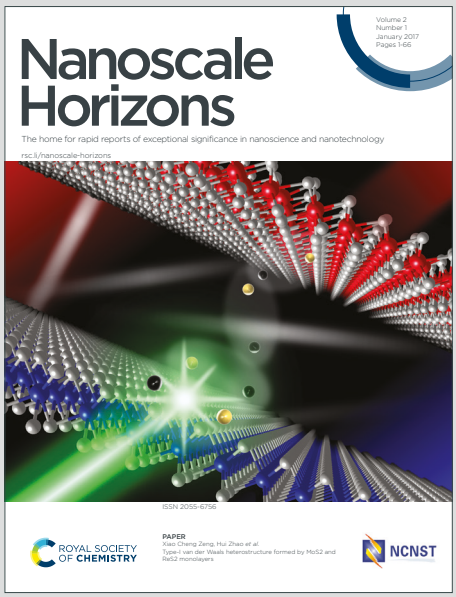

View Article Online
DOI: 10.1039/D0NH00098A

New Concepts

Microwave sensors based on microstrip antenna are good candidates for wearable devices due to their far field wireless communication feature without battery requirement. However, current microstrip technology cannot meet the demand for epidermal testing, which requires higher sensitivity. In this work, for the first time, we proposed and demonstrated nanostrip antenna based microwave sensors. Following the metamaterial design, the ordered nanostrips array, composed of conductive polymers, which are fabricated by low cost nanoscale printing approach, shows a strong enhancement of microwave signals. We further constructed a novel microwave enzymatic biosensor based on nanostrips doped with glucose oxidase. The proposed sensor shows a high performance for glucose sensing with low detection limit, wide dynamic range, and fast response. By integrating the nanostrips on flexible substrate, it demonstrated as a wearable epidermal biosensor for sweat glucose sensing. The proposed new type of nanoscale microwave biosensor could be applied as a general platform for the ultra-sensitive detection of various biomarkers.

View Article Online
DOI: 10.1039/D0NH00098A

COMMUNICATION

Nanostrip Flexible Microwave Enzymatic Biosensor for Noninvasive Epidermal Glucose Sensing †

Received 00th January 20xx,
Accepted 00th January 20xx

DOI: 10.1039/x0xx00000x

Qiannan Xue,[#a] Zheyu Li, [#a] Qikun Wang,[a] Wenwei Pan,[a] Ye Chang [a] and Xuexin Duan*[a]

Microwave sensors based on microstrip antennas are promising as wearable devices because of their flexibility and wireless communication compatibility. However, their sensitivity is limited due to the reduced sensor size and the potential of biochemical monitoring need to be explored. In this work, we present a new concept to enhance the microwave signals using of nanostrip-based metamaterials. The introduction of the nanostrip structures were achieved by theory and simulations. Experiments proof their enhancement to the electric field and sensing response in the characteristic gigahertz (GHz) wave band. Ordered nanostrips were fabricated on plastic substrate through simple nanoscale printing approach. Glucose oxidase is directly doped into the nanostrips, which enables a flexible wearable enzymatic biosensor for glucose sensing. Sensing experiments demonstrated that the nanostrip biosensor gives excellent performance for glucose detection, including high sensitivity, fast response, low detection limit, high affinity, and low power consumption. The applicability of the nanostrip-based sensor as wearable epidermal device for real-time noninvasive monitoring of glucose in sweat is verified as well.

Introduction

Developing epidermal electronic devices based on skin-friendly soft elastic materials has been of great interests over the past several decades. Due to their body compliance, when attached to the human skin, these flexible devices can be applied as wearable sensors to provide useful human health and medical information of individuals[1, 2]. Early efforts in developing these flexible and wearable sensors are focused on monitoring body physical signals such as steps[3], pulse wave[4], voice[5], motion[6], breath[7, 8], heart rate[9] and skin temperature[10]. Different types of transducers including force[11], pressure[12, 13], temperature[14], and humidity[15, 16] sensors have been reported. Recently, flexible and wearable biosensors have been proposed as well.[17] Compared to physical sensors, these devices require integration of specific bioreceptors into sensing elements which are capable of recognizing target analytes in complex samples at physiologically relevant concentrations[18]. Due to their conformal contact with the skin, such flexible epidermal biosensors can achieve in situ analysis of the biomarkers in the body fluid such as sweat and interstitial fluid. This provides clear advantages compared with conventional blood test, where invasive blood collection is inevitable. Though many biomarkers could be detected by such wearable biosensors, current researches focus largely on minimally invasive glucose monitoring, which is driven by the huge glucose sensing market for therapeutic diabetes applications. To enable the continuously glucose monitoring, entrapment of the enzyme glucose oxidase within the flexible device is generally required. Different types of transducers including electrochemical[19], optical[20] and piezo-electrical[21] sensing devices have been reported. Though the sensing element of these flexible biosensors has been largely optimized, one of the challenges for real-life application of these wearable epidermal electronics are that need complex data processing circuit and wireless transmission module, which are difficult to be flexible really. Finding an alternative sensing method which could facilitate the data processing and transmission and compatible with flexible device design may provide a new avenue.

In recent years, microwave biochemical sensor which is based on the change of electromagnetic properties of the sensing materials at ultrahigh frequencies (ca. >1 GHz) has been emerged[22]. In the presence of electromagnetic waves, microwave sensor exhibit a strong resonance behaviour with the samples under test[23]. The resonant frequency and magnitude will be shifted according to the content and concentration of the sample. Owing to the features of high frequency and passive conduction, microwave sensing technology is very suitable for matching with high frequency wireless transmission circuit, or as a part of antenna system, so that the required processing and data transmission circuit could be greatly simplified[24, 25]. In particular, microstrip type of microwave sensors can be designed as planar electrodes, which are compact, mass-produced and can be fabricated on various substrates using low cost screen printing technique[26].

[a] State Key Laboratory of Precision Measuring Technology & Instruments, School of Precision Instruments and Optoelec-tronics Engineering, Tianjin University, Tianjin 300072, China.
Email: xduan@tju.edu.cn

† Electronic Supplementary Information (ESI) available: See DOI: 10.1039/x0xx00000x

View Article Online
DOI: 10.1039/D0NH00098A

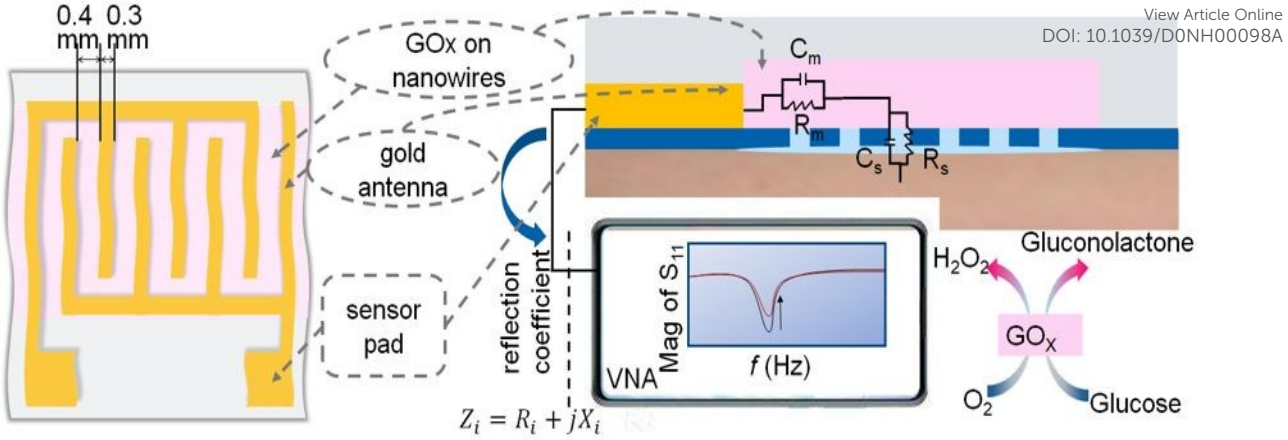

Figure 1. Schematic illustration of the sensing mechanism and measurement setup.

Such sensors have been demonstrated for wireless monitoring of temperature[27] and humidity[28]. Biochemical sensing using microstrip antennas such as for water-ethanol mixtures[29], milk adulteration[30], cells[31] and cancer biomarkers[32] detections have been reported as well. Very recently, flexible microwave sensor has been developed to enable the conform contact to the target[33]. Mason and Korostynska *et. al.* presented a very first example using of flexible microwave sensor for lactic acid monitoring as a functional wearable system.[34] However, the detection limit due to the sensor size reduction hinders the performance of current microstrip based wearable sensing system. The response signal and trace detection ability of microwave sensor for biochemical index need to be improved.

According to the electromagnetic enhancement mechanism, roughening of a metal surface, can enhance the resonance caused by excitation of electromagnetic waves, which will greatly improve the electric field intensity. A typical representative is metamaterial, which is defined as the electromagnetic material arranged periodically and its size is smaller than the wavelength of the incident electromagnetic wave[35]. The metamaterial can manipulate electromagnetic wave by dedicate design of its structure, which has been demonstrated for improvement of the sensing performance of electromagnetic wave sensing[36]. Studies on metamaterials have expanded to a fairly broad electromagnetic spectrum[37], including infrared chemical analysis[38], terahertz imaging[39] and microwave nondestructive evaluation[40]. Inspired by these studies, in this work we proposed a nanostrip type of metamaterial to enhance microwave biosensing based on sub-100 nm ordered conductive polymer nanowires array (Figure 1). The design of the nanostrips is analyzed by theory and simulations to enable a strong localization and enhancement of the electromagnetic field. The nanostrips were then fabricated on a flexible plastic substrate by a nanoscale soft printing approach featured with facile fabrication/manufacture with high throughput [41]. The GOx enzyme was directly doped into the nanostrips with biotin-streptavidin conjugation to enable a specific glucose sensing. Such flexible epidermal biosensor was tested for glucose detection after attachment to human skin at different bending conditions. Though this work only demonstrates for glucose sensing, the proposed new type of nanoscale microwave wearable biosensors can be applied as a general platform for different biomarker detections when integrated with other bio-probes. It has potential application prospects in biomedical testing where low detection limit is required[42].

Results and discussion

Mechanism and the enhancement effect of the nanostrip. As shown in Figure 1, the nanostrips are composed of continuously conductive polymer nanaowires, which contacted with the interdigital microwave antenna. The nanostrips integrated microwave sensor is connected with a miniaturized vector network analyzer (VNA) through a subminiature version A interface to extract the microwave spectrum and the reflection coefficient, S_{11}, can be tested in real time[26]. The measured value of the input impedance, Z_i, at the target frequency is extracted from the S_{11}.

$$S_{11} = \frac{Z_i - Z_0}{Z_i + Z_0} \quad (1)$$

$$Z_i = \sqrt{\frac{\mu_0\mu}{\varepsilon_0\varepsilon}} \tanh\left(j2\pi f\sqrt{\mu_0\mu\varepsilon_0\varepsilon}d\right) \quad (2)$$

where f and d are the frequency of the microwave and the thickness of the nanostrips, respectively. j represents the imaginary part. μ and ε are the relative complex permeability and the relative complex permittivity of the nanostrips[43]. As described in literature[44], the complex permeability is mainly related to the properties of the material itself, thus the changes caused by the configuration of the antennas are not significant. However, the equivalent complex dielectric constant could be changed by the different configuration of the antenna, which indicates the introduction of 1D nanoscale structures may greatly affect the equivalent impedance and the microwave signal.

Next, we discussed the performance of nanostrip-based sensor, and analyzed the expected enhancement effect of the nanostrips compared with the conventional microstrip sensor by simulations. Figure 2a&2b show the electric field distribution of the nanostrips and microstrips antennas (the local electric field distribution is shown in Figure S1). According to the results, the electric field distribution of nanostrips antenna is significantly stronger than that of microstrips, which is

View Article Online
DOI: 10.1039/D0NH00098A

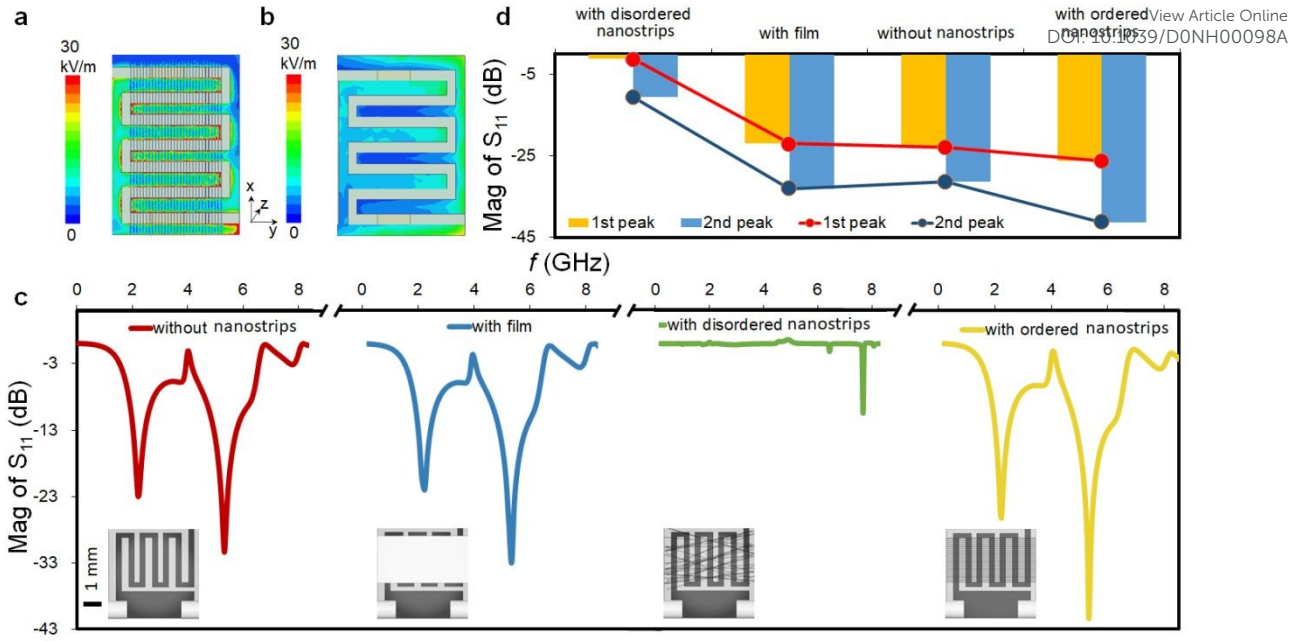

Figure 2. Electric field distribution of the proposed sensor with microstrips a) and nanostrips b) at the characteristic frequency; simulated reflection coefficient of the microwave biosensor without nanostrips, with thin film, with disordered nanostrips and with ordered nanostrips c); corresponding peak value of S_{11} magnitude spectrum of the four microwave sensors d).

ultimately reflected in an increase in the overall electric field strength. This is due to the fact that the nanoscale line width of nanostrip increases the local current density and ultimately leads to an increase in the electric field strength. This result consists with published reports, where they showed that improving the electric field strength by the one dimensional nanostructures[45, 46]. The stronger the electric field, the greater the change in the degree of polarization of the measured object, and thus it is easier to reflect into the change of microwave signal.

The spatial distribution of the nanostrips and its effects to the microwave response signal were further analyzed. The reflection coefficient magnitude of microstrip antennas without nanostrips, with a conductive polymer thin film (same height with the nanostrips), with disordered nanostrips, and ordered nanostrips were simulated, separately (Figure 2c). The simulation results show that four kinds of antennas all have characteristic peaks at 2.2GHz and 5.3GHz. The ordered nanostrips antenna obtained the maximum response (Figure 2d) at the two frequencies. The thin film coated microwave sensor though has a same height with the nanostrips has almost no enhancement effect. It is also interesting to note that the reflection coefficient magnitude of the microstrip antennas with the same nanostrips but disordered shows the smallest signal. This indicates that the introduction of nanomaterials needs to be as an orderly arrangement to present the enhancement effect. This result agrees with the published report that the microwave peak will be higher with the parallel nanowires due to the array layout shape[44]. Such effect is also consistent with the properties of metamaterials for electromagnetic wave manipulation, where the periodic 1D nano-structure with sub-wavelength size has the strongest enhancement effect on the local electric field[47]. For one-dimensional line structure with parallel arrangement, κ can be used to represent the resonance in the same direction as the applied electromagnetic wave. It can be expressed as[48, 49]:

$$\kappa = \frac{1-q}{q} \quad (3)$$

$$q_x = \frac{1-e^2}{e^2}\left[\frac{1}{2e}\ln\left(\frac{1+e}{1-e}\right) - 1\right] \quad (4)$$

$$e = \sqrt{1-\left(\frac{D^2}{L^2}\right)} \quad (5)$$

$$q_y = q_z = \frac{1-q_x}{2} \quad (6)$$

where D is the width of nanowire, L is the length of nanowire, and q *and* e are factors which depends on the length of the nanowire. It can be seen from Eq (3) - (5) that D and L are the two key factors, the larger the length-width ratio (L/D) of nanowires is, the higher of the resonance factor κ_x is, and it will result a greater resonance. $\kappa_y = \kappa_z$ corresponding to the resonance in the direction perpendicular to the electromagnetic wave, where it shows little effect on the transmission direction of microstrip line. In this paper, parallel nanowires are aligned in a large area, with a length larger than 0.4 mm and a linewidth less than 100 nm thus, L/D > 4000. By comparison, thin film and disordered nanowire structures both have relatively low L/D ratio. On account of these reasons, the scale of nanowires is much smaller than the wavelength and with a high L/D ratio, thus, the nanostrips sensor with ordered nanowires exhibits a stronger resonance and yields higher magnitude response compared to the microstrips without nanowires or with disordered nanowires. These results agree with the simulated electric field (Figure 2a&2b, Figure S1), which proves that the introduction of the ordered nanostrips based metamaterial can produce higher microwave response signal.

View Article Online
DOI: 10.1039/D0NH00098A

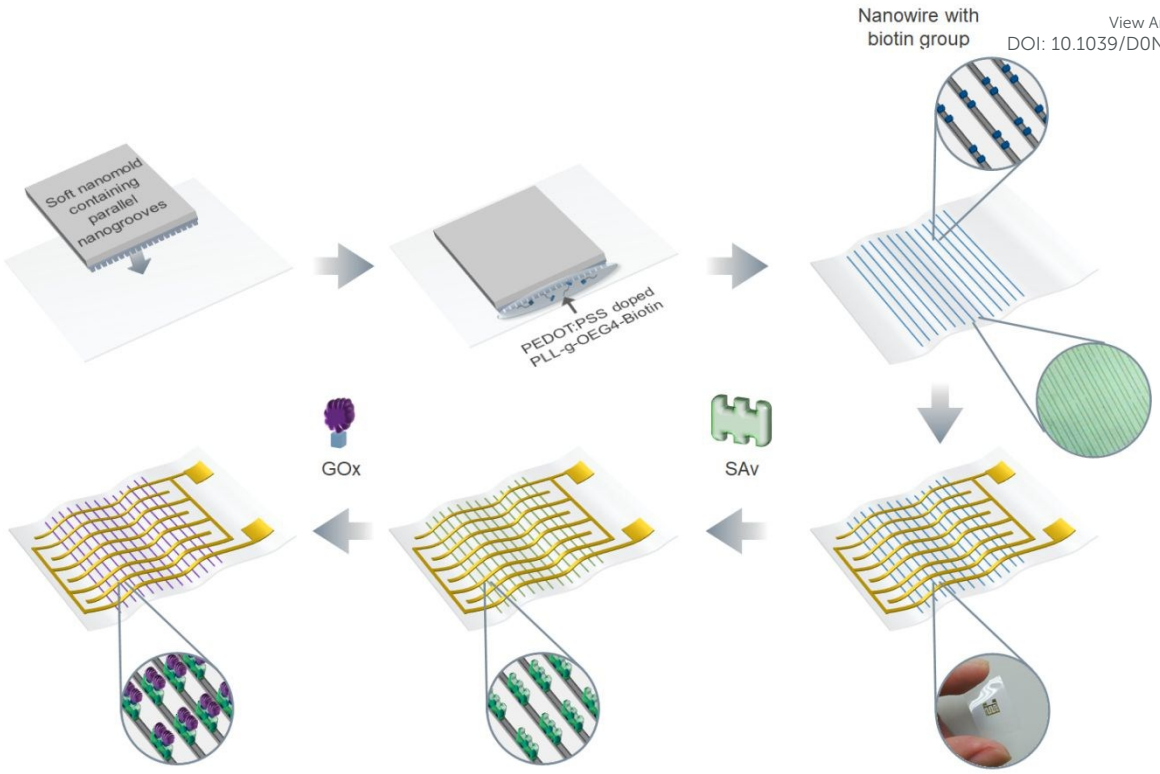

Figure 3. The schematic of the proposed nanostrip biosensor fabrication and enzyme immobilization

To enable the specific glucose sensing, GOx enzyme was immobilized into the nanowires of the proposed microwave sensor. When exposed to glucose sample, the reaction of the GOx enzyme and glucose produces gluconolactone (lactone of gluconic acid) and hydrogen peroxide (H_2O_2) according to the following reactions.

$$Glucose + GOx_{(oxd)} \rightarrow Gluconolactone + GOx_{(red)} \quad (7)$$

$$GOx_{(red)} + O_2 \rightarrow GOx_{(oxd)} + H_2O_2 \quad (8)$$

As an enzyme, GOx can be reused as the reaction reaches equilibrium, and the product concentrations change as a result. The incorporation of GOx ensures that any concentration change in the environment is specifically related to the presence and amount of glucose in a given sample. The concentration changes will result a variation in the dielectric constant, which can be detected by the microwave sensor. The equivalent dielectric constant[50] is equal to

$$\varepsilon_{eff} = \frac{\varepsilon_m + \varepsilon_s}{2} + \left(\frac{\varepsilon_m - \varepsilon_s}{2}\right)\left(\frac{1}{\sqrt{1+12d/w}}\right) \quad (9)$$

where *d* and *w* are the height and width of the substrate. ε_m and ε_s are the dielectric constants for the substrate and the glucose sample, respectively. Under a microwave field, changes in the dielectric constant of the measured sample is directly related to the changes in the impedance, which can be detected by the microwave sensor.

Fabrication and characterizations of the nanostrip microwave biosensor. The fabrication and functionalization of the nanostrip flexible microwave biosensor is shown in Figure 3. The nanostrips were first patterned by nanoscale soft-printing (NSP) directly on polyethylene terephthalate (PET) substrates. The NSP approach relies on the conformal contact between the soft mode (PDMS) containing nanogrooves structures with the bottom substrate. The formed nano-channels ensure the rather large Laplas pressure, which enables the facile filling of the channels with aqueous inks through simple capillary filling. The NSP can be applied to many different substrates featured with simple operation and without cleanroom facilities. According to theory analysis, narrower nanowires, higher density of the nanowires are preferred to achieve the maximum microwave enhancement effect (see supporting information S1), we still need to consider the limitation of the materials and fabrication cost of the nanowires. The typical size of PEDOT: PSS nanoparticle domain is about 60 nm[51], the line width of 100 nm ensures that the PEDOT:PSS can form continuous 1D nanowires without clogging. Regarding the distance between the neighbored nanowires, higher density of the nanowires will increase the cost of the nanomold. Besides, if the space between the neighbored nanowires is too short, it cannot achieve good conformal contact between the PDMS mold and the substrate, which will result leaking of the PEDOT:PSS solution during the capillary filling and significantly reduce the quantity of the nanowires. Considering the intensity of the absorption peak did not change too much in the range of sub-10 micrometer space between the neighbored nanowires (Figure S1e&f), we used the averaged 4 μm spacing in this work. Overall, the designed template contains parallel nanogrooves with a cross section of 100 nm (width) × 60 nm (depth) and the spacing between the neighbored nanogroove is 3 μm and 5 μm. To enable the bio-functionalization, here, a mixed conductive polymer aqueous ink is designed by mixing of positively charged polymer (PLL-g-OEG4-Biotin) with the negatively charged PEDOT:PSS at a typical mixing ratio at 1:9[41, 52].

View Article Online
DOI: 10.1039/D0NH00098A

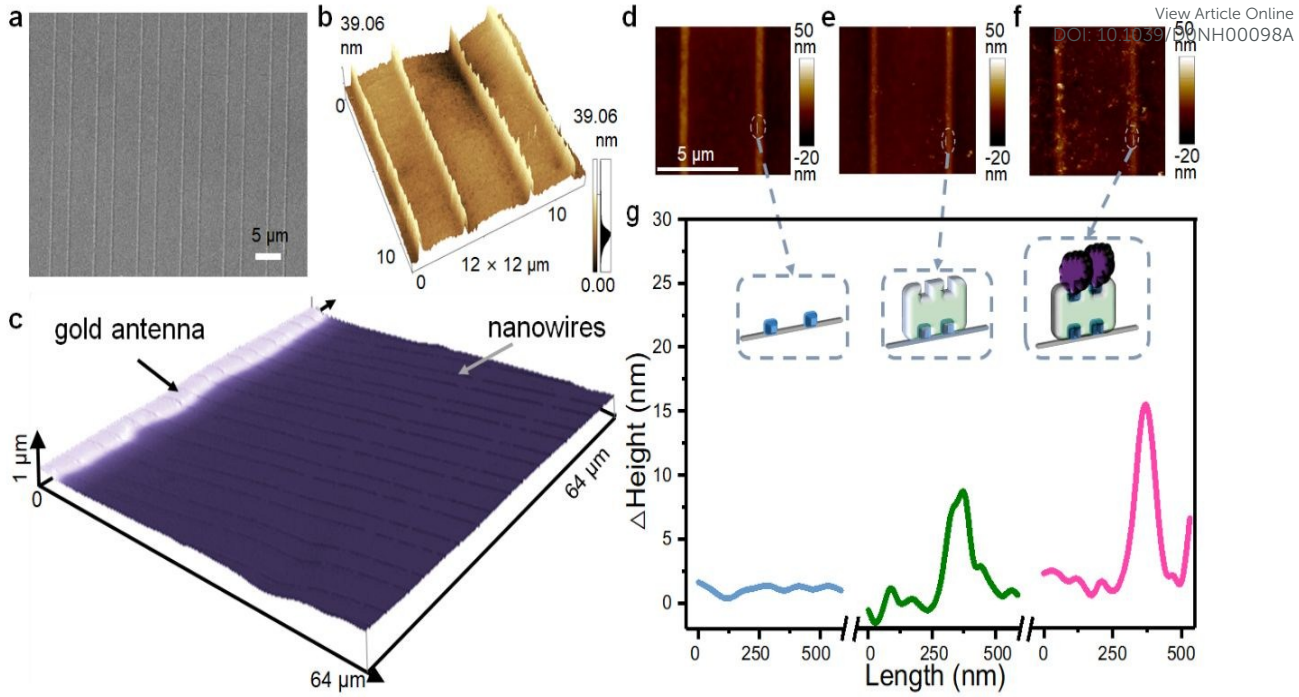

Figure 4. Surface morphology analysis of the nanowires fabricated on PET substrate by SEM a), AFM b) and confocal microscopy c); the AFM height images of the original nanowires d), after SAv modification e), and after GOx immobilization f); the extracted height information of the nanowires before (blue line), after SAv modification (green line), and after GOx immobilization (pink line) g).

The molecular structure of PEDOT:PSS doped with PLL-g-OEG4-Biotin is given in Figure S2a. Such molecular design ensures the good conductivity of the nanowires and direct doping with biotin. After biotinylated nanowires structurally patterned, the interdigital antenna structure was deposited graphically with gold evaporation through a shadow mask. Finally, glucose oxidase (GOx) was immobilized on the nanowires through biotin-SAv conjugation. Therefore, the nanoscale glucose microwave biosensor was fabricated, which based on nanowires linked GOx enzyme directly.

Scanning electron microscopy (SEM) (Figure 4a) and optical microscopy (Figure S3a) images show that the nanowires are collimated and orderly arranged on the transparent PET substrates. The atomic force microscopy (AFM) (Figure 4b) image shows that the nanowires are firmly adhered to the substrate and aligned parallel with each other with the height of 39 nm, width of 100 nm and distances between the wires alternating between 3 and 5 μm, which is consistent with the template. After metal evaporation, the nanowires were further checked by laser confocal microscopy and electrical characterization. As shown in Figure 4c, the nanowires are arranged vertically with the gold antenna, aligned on the flexible substrate uniformly. The IV curve of the conductive nanowires is straight and presents as a typical ohmic characteristics with a typical resistance around 0.3MΩ (Figure S3c). Next, we used AFM to follow the enzyme immobilization process on the nanowires. Before the introduction of proteins, the surface of nanowire is smooth (Figure 4d). After SAv and enzyme modification, granular protrusions were observed on the nanowires, and the particle height increased after the GOx enzyme immobilization (Figure 4e, f). The cross section analysis shows the height of the nanowires are 1.6 nm (original), 10.8 nm (after SAv modification) and 16.1 nm (after GOx immobilization) (Figure 4g). The height differences coincide with the size of SAv and GOx. Further observation by laser confocal microscopy (Figure S4a&S4b), the average height of nanowires before and after the immobilization of GOx by biotin–SAv conjugation was increased by 17.3 nm, which is also consistent with the results of AFM.

The microwave spectrum of the nanostrip sensor after SAv and GOx immobilization are shown in Figure S5. After SAv and GOx binding, the S_{11} magnitude both increased. This is caused by the immobilization of the proteins, which increase the equivalent impedance of the nanowires.

The results of SEM, AFM, laser confocal microscopy, and microwave spectrum confirm the highly ordered nanowires are patterned on the flexible PET substrate firmly and uniformly. The proteins have been successfully immobilized on the nanowires as well.

Glucose measurement. The proposed nanoscale microwave biosensor was used to detect different concentrations of glucose (Figure 5a). The sensor was exposed to the sample without glucose and with three different concentrations of glucose at 0.1 nM, 10 nM, and 1 μM in turn. The S_{11} magnitude response decreased accordingly, and the glucose content in the low concentration range can be clearly distinguished by the proposed sensor. The decreased of the S_{11} value upon increased glucose concentration is due to the fact that under the catalysis of GOx enzyme, the content of hydrogen peroxide in the solution increases, thus increasing the dielectric constant of the solution and decreasing the microwave peak. The above results also show that the characteristic glucose sensing frequency

View Article Online
DOI: 10.1039/D0NH00098A

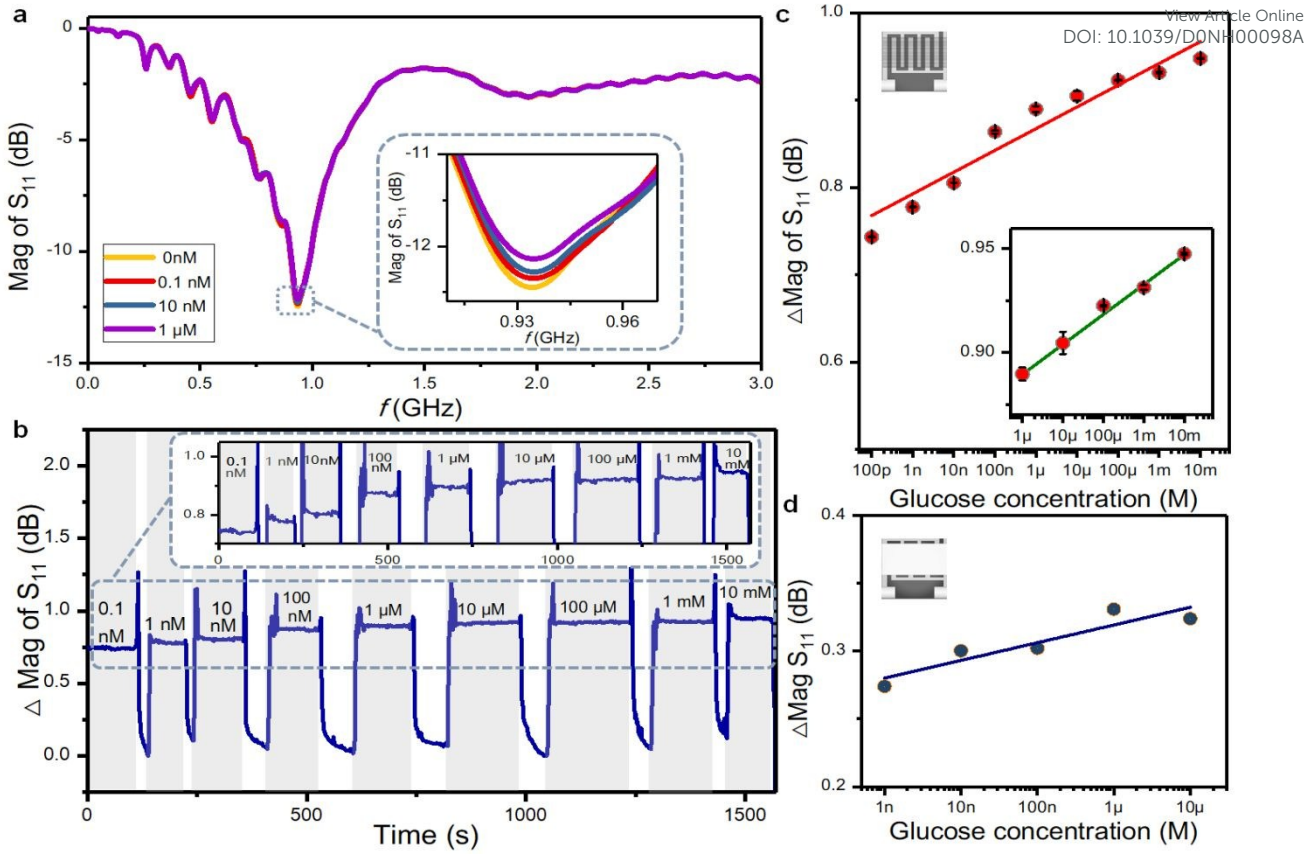

Figure 5. Reflection coefficient spectra of the proposed nanostrip sensor before and after contacted with four different concentrations of glucose a); Real-time glucose detection from 0.1 nM to 10 mM b); relationship between response of the nanostrips-based microwave biosensor and glucose concentration c); relationship between response of the film-based microwave biosensor and glucose concentration d)

range is 0.9–2.0 GHz, and the peak value of S_{11} magnitude is collected in real time at this frequency range. Figure 5b shows the time dependent glucose measurement, that the response value changes regularly with increasing concentration from 0.1 nM to 10 mM glucose solutions.

The ability of the sensor to return to the baseline was also tested. Based on five measurements after the removal of each glucose solution, the baseline is -13.1dB with the standard deviation of 0.18%. There was very little difference in the measured values after removing the solution, indicating that the sensor has a stable baseline and small drift, which are essential for real-time sweat monitoring. We further tested the long-term stability of the sensor by measuring glucose concentrations of 0.1 nM, 10 nM, and 10 μM for 10, 50, and 100 min, respectively, and the differences are 0.25%, 0.67% and 0.43%. The experimental results show that the sensor can function stably for long periods in the presence of a glucose solution with a small drift (Figure S6).

We then characterized the dynamic response of the biosensor. After the addition of a glucose solution, the response magnitude of the biosensor increases rapidly with a fast response, which indicates the operating speed of gigahertz band is quickly enough to meet the requirement of monitoring the chemical reaction[53, 54]. The typical Michaelis-Menten kinetics were observed as characterized by a gradually increase in the response loss up to the concentration of saturation (Figure S7)[55]. Michaelis Constant, k_m is calculated as 4.6×10^{-2} μM, which is lower than that of the glucose sensor based on optical fiber method (5.99×10^{-2} μM)[56], microelectrode method (0.28 mM)[57], and gel film method (30 mM)[58]. A lower value of k_m is deemed to be a higher catalytic activity of the immobilized enzyme[55]. The results show that the proposed nanostrips biosensor doped directly with GOx enzyme possess high affinity for glucose. Referring to the reaction-diffusion theory, the geometry of the nanostrips ensures a higher diffusion rate than that of planer microstrips[59], thus facilitates the contact between the immobilized enzyme and the glucose in solution. Besides, uniformed distribution of GOx doped on highly ordered nanowires, nano-scale linewidth and micro-size spacing make provides large reaction area with low steric hindrance, resulting a high catalytic affinity.

Figure 5c plots the S_{11} magnitude changes to the logarithm of glucose concentrations, which clearly presents a linear response from 0.1 nM to 10 mM with a sensitivity of 0.026 dB/log (nM). Within a glucose concentration range of 1 μM to 10 mM, the response linearity reached 0.992. We also compared the sensor response with the thin film-based microwave biosensor at the same glucose concentration (Figure 5d). The polymer thin film was prepared by spin coating the same polymer ink composed of PEDOT:PSS and PLL-biotin, which has a typical thickness at ~100 nm. In principle, the thin-film based microwave biosensor contains more GOx compared

View Article Online
DOI: 10.1039/D0NH00098A

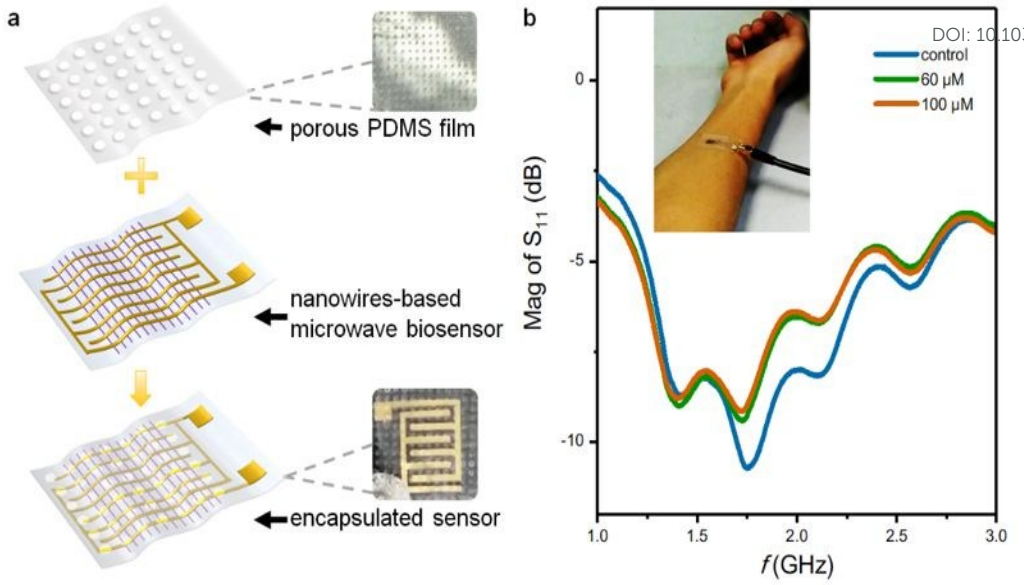

Figure 6. Packaging process with PDMS porous membrane a); microwave spectrum from sensor attached to skin b).

with the nanostrip sensor. However, the calculated sensitivity of the thin film-based microwave biosensor (0.013 dB/log (nM)) is only half of the nanostrip sensor. Besides, the nanostrip microwave sensor has better linearity and larger dynamic working range.

Figure S8 shows the reflection coefficient spectrum of the film-based microwave sensor, with peak lower than that based on nanostrips. These results confirm that the introduction of nanostrips, as a periodic nanostructured metamaterial, effectively enhances the resolution of the measured samples in the microwave frequency band.

To test the nanostrip sensor response in real complex sample, we prepared a simulated sweat solution (0.1% sodium dihydrogen phosphate, 0.5% sodium chloride, 0.5% lactic acid, 0.1% urea, and different concentrations of glucose in ultrapure water, pH adjusted to 5.5 with NaOH[60]). Two glucose concentrations of 10 nM and 1 μM were measured with the nanostrip sensor. The concentrations measured by the sensor were 9.5 nM and 1.012 μM, respectively, representing accuracies of 95.3% and 101.2%. Then, the sensor was placed in several possible interfering substances for interference testing. As shown in Figure S9, the response of the sensor to glucose is much higher than the others. Table S1 compares the performance of the nanostrip sensor with previously reported glucose measurements with other type of sensors. The nanoscale microwave biosensor reported herein exhibits a wider test range, shorter response time, and lower detection limit, reflecting the superiority of the sensor performance.

Epidermal sensing. One of the objects in developing flexible biosensors is for epidermal sensing applications, where flexible substrate ensures the conform contact to the skin. We then tested the device bending effect on its sensing performance.

The nanostrip sensor was bent to 36 ° to simulate the curvature arising from attachment to the human body, then placed in 0.1 nM, 10 nM, and 1 μM glucose solutions and tested in turn. As shown in Figure S10, the microwave spectrum of the bended sensor has a slightly positive frequency shift and a decrease in response value compared with the flat sensor. However, its response still effectively distinguishes trace concentrations of glucose, and it is consistent with the response trend with the flat sensor. As the physical disturbance can induce changes in the magnitude and frequency of the microwave, the proposed sensor is more suitable for attaching to the relatively static parts of the body, such as backside[61], where complex bending or twisting situation is not likely to happen. In the following study for practical application, the interference caused by slightly mechanical disturbance should be considered, for example, introducing bending correction algorithm[62]. Under a fixed curvature, the sensor shows a rather good performance for glucose sensing with high linearity (Figure S11) and the detection limit (LOD) is calculated as 0.1 nM. Currently, blood glucose measurement is still the gold standard for glucose monitoring. Some recent studies have proofed that the sweat glucose measurement is a compromise method, which features with no invasive[63]. However, due to the fluctuation of the glucose level in real sweat, here we chose a simulated sweat sample containing spiked glucose as a test sample to prove the feasibility of the propose nanostrip sensor for wearable glucose measurement[60, 64]. A porous polydimethylsiloxane (PDMS) film with a typical thickness of 281.8 μm and hole diameter of 200 μm was prepared to encapsulate the sensor (Figure 6a). The porous thin film acts as a passivation layer to prevent signal interference[65], and provides a micro chamber for the catalytic reaction (Figure S12). The packed flexible epidermal glucose biosensor was then attached to the human skin, and the microwave spectrum of the sensor was monitored in real time using a miniaturized VNA with a typical size at 9 × 8.3 × 1.4 cm^3 and a tablet (Figure S12d). In principle, a wireless signal-reading circuit and miniaturized VNA chip[66] could be developed as an alternative to further miniaturize the detection system.

As shown in Figure 6b, after the sensor attached to the skin, obvious resonance peaks can be observed in the frequency

View Article Online
DOI: 10.1039/D0NH00098A

range of 1.0 - 2.0 GHz. Two concentrations of simulated sweat (60 μM and 100 μM[67]) were used, representing the glucose levels of sweat before and after meal, respectively. After the samples were added between the skin and sensor patch, the peak value of the sensor immediately decreased with the increase of glucose concentration. This result proofs the sensor can distinguish the glucose concentration from simulated sweat when attaching to human skin. It is also noted that the peak value of microwave signal is slightly weaken after contacted to the skin which is likely due to the attenuation of the electromagnetic wave in the lossy tissue. Though the sensor can still response well to the glucose concentration change, a ground plane can be integrated in the sensor to prevent the absorption.

Conclusions

This paper reported a flexible epidermal microwave biosensor integrated with nanostrip structures. The ordered nanostrips fabricated by nanoscale printing approach strongly enhanced the microwave signals which are proved by simulation and experiments. The GOx enzyme were further integrated into the nanostrips for specific glucose sensing. The sensing results proof that the nanostrip structures not only enhance the electric field of the microwave but also ensure the high performance of glucose sensing, such as high sensitivity, fast response, high catalytic affinity, and low power assumption, which is due to the high surface-to-volume ratio and extremely small configuration of the nanostrips. The nanostrips-based microwave sensors are further prepared as epidermal glucose biosensor, which is capable of conformal contact with skin and non-invasive real-time monitoring of sweat glucose.

Experimental

Materials and Reagents. Polydimethylsiloxane (PDMS) was prepared by SYLGARD 184 SILICONE ELASTOMIER. Poly-L-lysine hydrobromide (PLL, MW ¼ 15 kDa - 30 kDa), Conducting polymer poly(3,4-ethylenedioxythiophene):poly(styrenesulfonate) (PEDOT:PSS), Lactic acid, Urea, and phosphate buffered saline (PBS, pH 7.4) tablets were purchased from Sigma & Aldrich. Streptavidin (SAv) was purchased from Aladdin Industrial Corporation (Shanghai, China). Sodium dihydrogen phosphate, sodium chloride was purchased from Tianjin Real&Lead Chemical Corporation (Tianjin, China). Biotinylated GOx was purchased from Tianjin Xiensi Corporation (Tianjin, China). All chemicals and solvents used were of analytical reagent grade and were used as received. Deionized water was used throughout the experiment. All analytes were diluted with 10 mM PBS buffer (pH 7.4) for variable concentrations.

Sensor Fabrication. First, well-defined soft nanogrooves were formed using a flat hybrid PDMS substrate, which was fabricated by thermal nanoimprint lithography[68]. The formed template was combined with a PET flexible substrate (3 mm × 3 mm). Thereafter, a mixing ink (PEDOT:PSS-doped PLL-*g*-OEG4-Biotin) with a special molecular design was applied between the template and substrate. The ink adhered to the silicon substrate according to the template shape and formed a uniform nanowire array with an average width of 100 nm and spacing between nanowires alternating between 3 and 5 μm. Next, a gold layer was deposited *via* thermal evaporation through a shadow mask with an interdigitated structure. Finally, SAv proteins were applied to the surface of the sensor and bound to the biotin groups of the nanowires through stable covalent bonds with two sites on one side of SAv. After 10 min of incubation, biotin-GOx was bound to the two sites on the other side of SAv that were available to connect to the nanowires and achieve enzyme immobilization. Using this method, the microwave biosensor based on a nanowire array with GOx was fabricated.

Instruments and Measurements. After fabrication, the sensor design consists of 50 Ω coplanar waveguide transmission line, then is packed with two port SMA connectors. The vector network analyzer (Keysight E5071C) was used to measure the sensor response to different glucose samples, and the changes of $|S_{11}|$ were observed in the GHz range. Finally, in the testing of sensor attachment to the skin, a miniaturized vector network (VNA 6000A, Xuanli Electronics Corporation, China) and a tablet were used.

Conflicts of interest

The authors declare no conflicts of interest.

Acknowledgements

Qiannan Xue and Zheyu Li contributed equally to this work. The authors gratefully acknowledge financial support from the National Natural Science Foundation of China (NSFC No. 61674114, 91743110, 21861132001), National Key R&D Program of China (2017YFF0204604, 2018YFE0118700), Tianjin Applied Basic Research and Advanced Technology (17JCJQJC43600), the 111 Project (B07014), the Initial Scientific Research Fund of State Key Laboratory of Precision Measuring Technology and Instruments, Tianjin University (No. Pilq1902), and the Foundation for Talent Scientists of Nanchang Institute for Micro-technology of Tianjin University.

Notes and references

1. W. Gao, S. Emaminejad, H. Y. Y. Nyein, S. Challa, K. Chen, A. Peck, H. M. Fahad, H. Ota, H. Shiraki, D. Kiriya, D.-H. Lien, G. A. Brooks, R. W. Davis and A. Javey, *Nature*, 2016, **529**, 509-514.
2. M. Poh, N. C. Swenson and R. W. Picard, *IEEE Trans. Biomed. Eng.*, 2010, **57**, 1243-1252.
3. F. Lin, A. Wang, Y. Zhuang, M. R. Tomita and W. Xu, *IEEE T. Ind. Inform.*, 2016, **12**, 2281-2291.
4. T. Yang, X. Jiang, Y. Zhong, X. Zhao, S. Lin, J. Li, X. Li, J. Xu, Z. Li and H. Zhu, *ACS Sens.*, 2017, **2**, 967-974.
5. P. Adhikary, A. Biswas and D. Mandal, *Nanotechnology*, 2016, **27**, 495501.

6. X.-G. Yu, Y.-Q. Li, W.-B. Zhu, P. Huang, T.-T. Wang, N. Hu and S.-Y. Fu, *Nanoscale*, 2017, **9**, 6680-6685.
7. P. Slobodian, R. Danova, R. Olejnik, J. Matyas and L. Münster, *Polym Adv Technol.*, 2019, **30**, 1891-1898.
8. N. Tang, C. Zhou, L. Xu, Y. Jiang, H. Qu and X. Duan, *ACS Sensors*, 2019, **4**, 726-732.
9. Y.-D. Lee and W.-Y. Chung, *Sens. Actuators, B*, 2009, **140**, 390-395.
10. Y. Yamamoto, D. Yamamoto, M. Takada, H. Naito, T. Arie, S. Akita and K. Takei, *Adv. Healthcare Mater.*, 2017, **6**, 1700495.
11. L. Viry, A. Levi, M. Totaro, A. Mondini, V. Mattoli, B. Mazzolai and L. Beccai, *Adv. Mater.*, 2014, **26**, 2659-2664.
12. M. Jian, K. Xia, Q. Wang, Z. Yin, H. Wang, C. Wang, H. Xie, M. Zhang and Y. Zhang, *Adv. Funct. Mater.*, 2017, **27**, 1606066.
13. Y. Chang, J. Zuo, H. Zhang and X. Duan, *Nanotechnol. Precis. Eng.*, 2020, **3**, 43-52.
14. W.-P. Shih, L.-C. Tsao, C.-W. Lee, M.-Y. Cheng, C. Chang, Y.-J. Yang and K.-C. Fan, *Sensors*, 2010, **10**, 3597-3610.
15. R. Alrammouz, J. Podlecki, A. Vena, R. Garcia, P. Abboud, R. Habchi and B. Sorli, *Sensor. Actuators, B*, 2019, **298**, 126892.
16. C. Zhou, X. Zhang, N. Tang, Y. Fang, H. Zhang and X. Duan, *Nanotechnology*, 2020, **31**, 125302.
17. C. Wang, K. Xia, H. Wang, X. Liang, Z. Yin and Y. Zhang, *Adv. Mater.*, 2019, **31**, 1801072.
18. Z. Zhang, M. Azizi, M. Lee, P. Davidowsky, P. Lawrence and A. Abbaspourrad, *Lab. Chip*, 2019, **19**, 3448-3460.
19. Y. Lin, M. Bariya, H. Y. Y. Nyein, L. Kivimäki, S. Uusitalo, E. Jansson, W. Ji, Z. Yuan, T. Happonen, C. Liedert, J. Hiltunen, Z. Fan and A. Javey, *Adv. Funct. Mater.*, 2019, **29**, 1902521.
20. S. Haxha and J. Jhoja, *IEEE Photonics J.*, 2016, **8**, 1-11.
21. X. Xue, Z. Qu, Y. Fu, B. Yu, L. Xing and Y. Zhang, *Nano Energy*, 2016, **26**, 148-156.
22. E. Porter, H. Bahrami, A. Santorelli, B. Gosselin, L. A. Rusch and M. Popović, *IEEE T. Med. Imaging*, 2016, **35**, 1501-1509.
23. G. Gennarelli, S. Romeo, M. R. Scarfì and F. Soldovieri, *IEEE Sens. J.*, 2013, **13**, 1857-1864.
24. J. Yao, S. Tjuatja and H. Huang, *IEEE Sens. J.*, 2015, **15**, 4338-4345.
25. X. Yi, T. Wu, Y. Wang, R. T. Leon, M. M. Tentzeris and G. Lantz, *Int. J. Smart Nano Mater.*, 2011, **2**, 22-38.
26. T.-G. Kang, J.-K. Park, G.-H. Yun, H. H. Choi, H.-J. Lee and J.-G. Yook, *Sens. Actuators, B*, 2019, **282**, 145-151.
27. D. Girbau, R. Á, A. Lazaro, S. Rima and R. Villarino, *IEEE Trans. Microwave Theory Tech.*, 2012, **60**, 3623-3632.
28. X. Wang, O. Larsson, D. Platt, S. Nordlinder, I. Engquist, M. Berggren and X. Crispin, *Sensor. Actuators, B*, 2012, **166-167**, 556-561.
29. X. Zhang, C. Ruan, T. u. Haq and K. Chen, *Sensors*, 2019, **19**, 787.
30. D. Agranovich, I. Renhart, P. Ben Ishai, G. Katz, D. Bezman and Y. Feldman, *Food Control*, 2016, **63**, 195-200.
31. Y.-F. Chen, H.-W. Wu, Y.-H. Hong and H.-Y. Lee, *Biosens. Bioelectron.*, 2014, **61**, 417-421.
32. H.-J. Lee, J.-H. Lee, H.-S. Moon, I.-S. Jang, J.-S. Choi, J.-G. Yook and H.-I. Jung, *Sensors and Actuators B: Chemical*, 2012, **169**, 26-31.
33. Q. Xue, X. Tang, Y. Li, H. Liu and X. Duan, *ACS Sensors*, 2019, **5**, 171-179.
34. A. Mason, O. Korostynska, J. Louis, L. E. Cordova-Lopez, B. Abdullah, J. Greene, R. Connell and J. Hopkins, *IEEE Trans. Biomed. Eng.*, 2018, **65**, 698-705.
35. T. Chen, S. Li and H. Sun, *Sensors*, 2012, **12**, 2742-2765.
36. Z. Jakšić, S. Vuković, J. Matovic and D. Tanasković, *Materials*, 2011, **4**, 1-36.
37. Z. Zhang, Z. Tian, C. Chang, X. Wang, X. Zhang, C. Ouyang, J. Gu, J. Han and W. Zhang, *Nanotechnol. Precis. Eng.*, 2018, **1**, 123-128.
38. Y. Li, L. Su, C. Shou, C. Yu, J. Deng and Y. Fang, *Sci. Rep.*, 2013, **3**, 2865.
39. H. Bilgin, S. Zahertar, S. Sadeghzadeh, A. D. Yalcinkaya and H. Torun, *Sens. Actuators, A*, 2016, **244**, 292-298.
40. Y. Zhang, J. Zhao, J. Cao and B. Mao, *Sensors*, 2018, **18**, 1912.
41. Q. Xue, Q. Wang, Z. Han, N. Tang, C. Zhou, W. Pan, Y. Wang and X. Duan, *Advanced Materials Interfaces*, 2019, **6**, 1970118.
42. S. Dalirirad and A. J. Steckl, *Sensors and Actuators B: Chemical*, 2019, **283**, 79-86.
43. M. Wu, H. He, Z. Zhao and X. Yao, *J. Phys. D: Appl. Phys.*, 2000, **33**, 2398.
44. Y. Chen, M. Cao, T. Wang and Q. Wan, *Appl. Phys. Lett.*, 2004, **84**, 3367-3369.
45. S. Jo, D. Banerjee and Z. Ren, *Appl. Phys. Lett.*, 2004, **85**, 1407-1409.
46. D. Banerjee, S. H. Jo and Z. F. Ren, *Adv. Mater.*, 2004, **16**, 2028-2032.
47. D. Shreiber, M. Gupta and R. Cravey, *Sensor. Actuators, A*, 2011, **165**, 256-260.
48. Y.-H. Ye, Y. J. Huang, W. T. Lu, B. D. F. Casse, D. Xiao, S. P. Bennett, D. Heiman, L. Menon and S. Sridhar, *Opt. Mater.*, 2011, **33**, 1667-1670.
49. B. G. McMillan, L. E. A. Berlouis, F. R. Cruickshank, D. Pugh and P.-F. Brevet, *Appl. Phys. Lett.*, 2005, **86**, 211912.
50. R. Liu, Z. Zhang, R. Zhong, X. Chen and J. Li, Texas Deparment of Transportation. Austin, 2007.
51. J. Zhou, D. H. Anjum, L. Chen, X. Xu, I. A. Ventura, L. Jiang and G. Lubineau, *J. Mater. Chem. C*, 2014, **2**, 9903-9910.
52. Z. Han, Y. Wang and X. Duan, *Analytica Chimica Acta*, 2017, **964**, 170-177.
53. H. Ito, F. Nakajima, T. Furuta and T. Ishibashi, *Semicond. Sci. Technol.*, 2005, **20**, S191-S198.
54. V. Rawat, S. Dhobale and S. N. Kale, *J. Appl. Phys.*, 2014, **116**, 164106.
55. T. Kong, Y. Chen, Y. Ye, K. Zhang, Z. Wang and X. Wang, *Sens. Actuators, B*, 2009, **138**, 344-350.
56. P. A. Raymundo-Pereira, F. M. Shimizu, D. Coelho, M. H. O. Piazzeta, A. L. Gobbi, S. A. S. Machado and O. N. Oliveira, *Biosens. Bioelectron.*, 2016, **86**, 369-376.
57. T. Yasukawa, K. Goto and F. Mizutani, *Electroanalysis*, 2010, **22**, 927-930.
58. A. Blandino, M. Maćias and D. Cantero, *Process Biochem.*, 2001, **36**, 601-606.
59. P. R. Nair and M. A. Alam, *Appl. Phys. Lett.*, 2006, **88**, 233120.
60. F. Wu, S. Zhang and Z. Tao, *Mater. Corros.*, 2011, **62**, 234-239.
61. M. E. B. Jalil, M. K. Abd Rahim, N. A. Samsuri, N. A. Murad, H. A. Majid, K. Kamardin and M. Azfar Abdullah, *Journal of*

View Article Online
DOI: 10.1039/D0NH00098A

View Article Online
DOI: 10.1039/D0NH00098A

Progress In Electromagnetics Research, 2013, **140**, 633-652.
62. F. Boeykens, H. Rogier and L. Vallozzi, *IEEE Transactions on Antennas and Propagation*, 2014, **62**, 1253-1260.
63. R. D. Munje, S. Muthukumar and S. Prasad, *Sens. Actuators, B*, 2017, **238**, 482-490.
64. J. D. Yuen, S. A. Walper, B. J. Melde, M. A. Daniele and D. A. Stenger, *Sci. Rep.*, 2017, **7**, 40867.
65. X. Xuan, H. S. Yoon and J. Y. Park, *Biosens. Bioelectron.*, 2018, **109**, 75-82.
66. J. Nehring, M. Dietz, K. Aufinger, G. Fischer, R. Weigel and D. Kissinger, *IEEE Transactions on Microwave Theory and Techniques*, 2016, **64**, 892-905.
67. J. Moyer, D. Wilson, I. Finkelshtein, B. Wong and R. Potts, *Diabetes Technol. Ther.*, 2012, **14**, 398-402.
68. B. D. Gates, Q. Xu, J. C. Love, D. B. Wolfe and G. M. Whitesides, *Annu. Rev. Mater. Res.*, 2004, **34**, 339-372.